Photoassociation spectroscopy of lattice-trapped ^{171}Yb atoms near the $^1S_0 - {}^3P_1$ $(f = 1/2)$ intercombination line

Changyue Sun,[1] Di Ai,[1] Taoyun Jin,[1] Tao Zhang,[1] Chengquan Peng,[1] Qichao Qi,[1] and Xinye Xu[1,2,3,*]

[1]*State Key Laboratory of Precision Spectroscopy, East China Normal University, Shanghai 200241, China*
[2]*Shanghai Research Center for Quantum Sciences, Shanghai 201315, China*
[3]*Shanghai Branch, Hefei National Laboratory, Shanghai 201315, China*

We report on the photoassociation (PA) spectroscopy of cold ^{171}Yb atoms in a one-dimensional optical lattice. The PA spectral lines correlating to the $^1S_0 + {}^3P_1$ $(f = 1/2)$ state are observed experimentally. High accuracy and narrow atom-loss spectra are measured ranging up to about 1.2 GHz red detuning with respect to the atomic resonance. The main systematic frequency shifts of the PA transitions are determined with total uncertainties less than 100 kHz, which is more accurate than previous similar experimental results. We determine the initial scattering state of the PA spectra by comparing the spectra with polarized and unpolarized atomic samples. By comparatively analyzing theoretical results calculated based on an adiabatic molecular potential with experimental data, the excited molecular potentials corresponding to the spectral lines are clarified. The precision measurement of the narrow PA spectra plays an important role in exploring atomic interactions and lays the groundwork for the study of cold ytterbium molecules.

I. INTRODUCTION

Photoassociation (PA) is the process of optically forming molecules from two colliding atoms [1]. The PA spectroscopy of ultracold atoms is a powerful tool to investigate long-range molecular states and determine the scattering length [2,3]. PA also provides a way to change the scattering length, which is called optical Feshbach resonance [4–7]. Furthermore, PA holds the potential to efficiently produce cold molecules [8–10] that are ideal candidates for applications ranging from quantum simulation to quantum sensing and metrology [11]. The molecules in the excited state decay into atoms, resulting in a detectable loss of atoms from an atomic trap, which provides a way to measure the PA spectroscopy. In a three-dimensional (3D) optical lattice, the PA process can be used to measure the number of atoms in doubly occupied sites and remove these atoms, which helps to realize a Mott insulator, and suppress the collision effect between atoms [12,13].

Ytterbium is a lanthanide element that has two electrons in its outermost shells with metastable states that have long lifetimes on the order of seconds. Cold ytterbium atoms have been widely studied in various fields, including optical clocks [14], quantum simulation [15,16], and quantum information [17,18], etc. Ytterbium has seven stable isotopes, including two fermionic isotopes with nonzero nuclear spin, specifically ^{171}Yb $(I = 1/2)$ and ^{173}Yb $(I = 5/2)$. PA spectroscopy of ytterbium has been observed for both bosons [2,3,19] and fermions [20,21]. The $^1S_0 + {}^3P_1$ intercombination transition has a narrow linewidth enabling high-resolution PA spectroscopy, and the optical Feshbach resonance using this transition is expected to be achieved

with less atom loss compared with the electric dipole transition [6,22]. High-resolution PA spectroscopy of ^{171}Yb near the dissociation limit of the $^1S_0 + {}^3P_1$ $(f = 3/2)$ transition has been measured, revealing the presence of hyperfine-structure-induced purely long-range states [20]. However, to date, the PA spectroscopy of ^{171}Yb near the $^1S_0 + {}^3P_1$ $(f = 1/2)$ transition remains unexplored.

In this paper, we present the experimental observation of PA spectroscopy of ^{171}Yb near the $^1S_0 + {}^3P_1$ $(f = 1/2)$ transition. Atom-loss PA spectra are measured in an optical lattice by scanning the frequency of the PA laser on the red-detuning side with respect to the atomic resonance. The main systematic frequency shifts and their uncertainties of the PA transitions are determined. We identify the initial scattering state of the PA spectra through comparing the spectra from polarized and unpolarized atomic samples. For spin-polarized atoms, the atom loss for PA resonance lines from the s-wave scattering state is suppressed while those from the p-wave scattering state remain unaffected by Fermi statistics. We specify the excited molecular potential associated with the spectral lines through a comparative analysis of experimental data and theoretical results. This investigation will contribute to our fundamental understanding and potential practical applications of the PA.

II. EXPERIMENT METHODS

The cold ^{171}Yb atoms are prepared in an optical lattice as described in Refs. [23,24]. The Zeeman-slowed atoms are first cooled and trapped using a two-stage magneto-optical trap (MOT) and then loaded into a 780-nm 1D optical lattice with a lattice depth of about $300E_R$, where E_R is the recoil energy. The schematic of the experimental setup is shown in Fig. 1. The atoms are trapped in a 1D tilted optical lattice
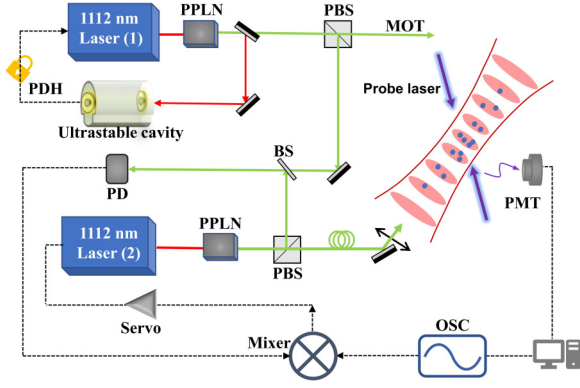

FIG. 1. Schematic of the experimental setup. Periodically poled lithium niobate (PPLN), photomultiplier tube (PMT), polarization beam splitter (PBS), photodetectors (PD), Pound-Drever-Hall method (PDH), and digital oscillator (OSC).

with a beam waist of 110 µm and the PA light with a beam waist of 750 µm irradiates along the same direction which could suppress Doppler broadening. Typically, 10^4 atoms are trapped in the optical lattice and the temperature is about 6 µK with an atomic density of about 10^{11} cm^{-3}. The 556-nm master laser used for the second stage MOT and spin polarization is locked to the ultralow expansion Fabry-Pérot cavity. Another 556-nm laser used for PA is referenced to the master laser. The superposition of the PA laser and the master laser is detected by a PD and gives rise to a beat signal at the difference frequency between them. The PD signal is mixed with the radio frequency (rf) from the reference oscillator followed by a low-pass filter to achieve the error signal. After the servo process, the PA laser locks to the master laser with a frequency offset similar to that of the reference oscillator. The linewidth of the PA laser is less than 10 kHz, which is much less than the molecular natural linewidth of $\Gamma_{nat} \approx 2\Gamma_a \approx 2\pi \times 364$ kHz [25], where Γ_a is the atomic linewidth of the $^1S_0 - {}^3P_1$ transition. After preparing cold ^{171}Yb atoms in the optical lattice [23,24], the PA light is applied to the atom and subsequently we obtain the PA spectra by measuring the remaining atom number. The frequency of the PA laser is scanned by controlling the frequency difference between the master laser and PA laser. Before applying the PA laser, we adjust the oscillator frequency via a remote computer (PC) and the PA laser frequency is immediately changed by the servo, while the laser remains locked. We obtain the PA signal by measuring the remaining atom number after the PA process in the optical lattice with the fluorescence method using the 399-nm $^1S_0 - {}^1P_1$ transition.

We get the PA detuning from the difference between the measured PA spectra and the measured atomic resonance spectroscopy under the same experimental conditions. Figure 2 shows the observed atom-loss PA spectra in which the measured frequency detuning is up to about -1.2 GHz. The frequency detunings and the linewidths of the PA spectra determined from Lorentzian fitting are listed in Table I. The achieved PA spectral linewidths are around a few hundred kHz, as detailed in Appendix B.

TABLE I. Characteristics of measured PA spectral lines and associated states in the $^1S_0 + {}^3P_1$ ($f = 1/2$) channel. v represents the vibrational quantum number counting down from the dissociation limit. T is the quantum number for the total angular momentum.

| Excited molecular potential state $\phi^\pm$	v	T	PA light shift) (MHz)	Light shift of resonance transition (MHz)	Temperature shift (MHz)	Density shift (MHz)	Statistic uncertainty (MHz)	PA frequency detunings ν_{expt} (MHz)	PA frequency detunings ν_{theor} (MHz)	Ground scattering states
0^+	7	1	−0.037(15)				0.006	−16.148(43)	−16.5	S
1	5	2	−0.017(7)				0.010	−18.789(42)	−19.2	P
1	5	1	−0.026(9)				0.010	−21.484(43)	−21.9	P
0^+	8	1	−0.025(2)				0.006	−34.930(41)	−35.6	S
1	6	2	−0.034(2)				0.029	−49.428(54)	−50.8	P
1	6	1	−0.037(8)				0.037	−54.026(55)	−55.4	P
0^+	9	1	−0.107(21)				0.013	−69.219(47)	−70.3	S
			0.043(4)				0.010	−79.900(42)		P
			−0.115(36)				0.030	−115.287(62)		S
1	7	2	−0.241(16)	−0.016(7)	−0.204(38)	−0.011(13)	0.031	−122.648(54)	−118.4	P
0^+	10	1	−0.212(12)				0.014	−128.049(45)	−129.8	S
0^+	11	1	−0.172(13)				0.007	−224.270(43)	−226.9	S
			−0.103(35)				0.028	−245.403(60)		S
1	8	2	−0.104(17)				0.018	−256.548(47)	−251.8	P
0^+	12	1	−0.132(10)				0.010	−375.234 (43)	−379.4	S
			0.205(37)				0.025	−484.477(60)		S
1	9	2	−0.327(30)				0.013	−500.466(52)	−496.2	P
0^+	13	1	−0.075(7)				0.009	−603.807(42)	−611.1	S
			−0.004(4)				0.015	−887.576(43)		S
0^+	14	1	−0.248(20)				0.003	−975.543(43)	−954.8	S
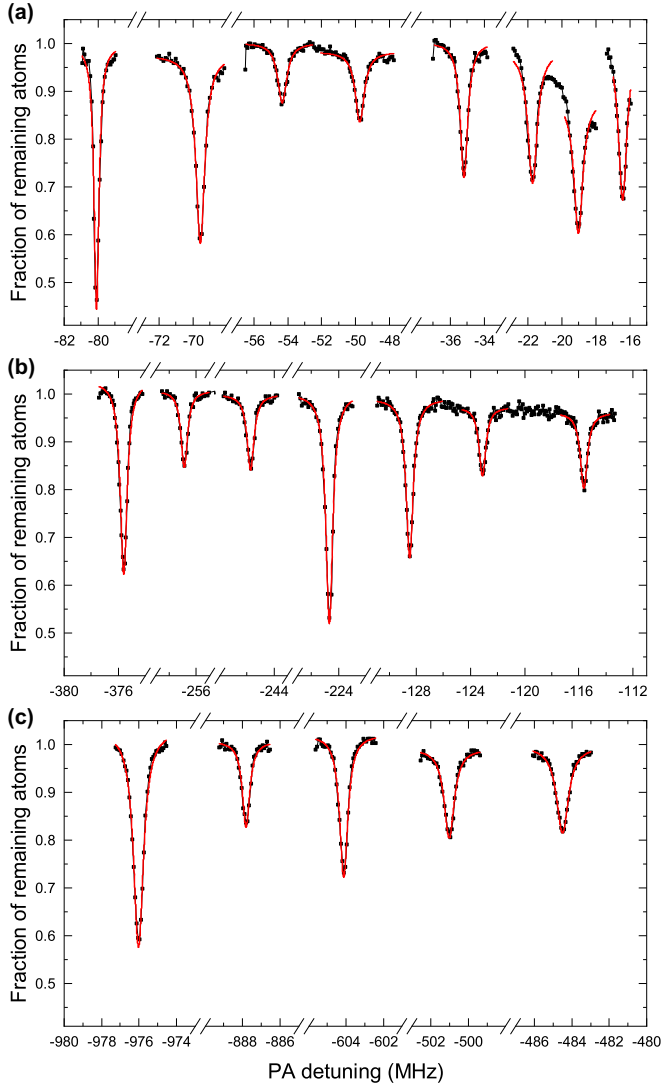
FIG. 2. PA spectra of ^{171}Yb atoms correlating to the $^1S_0 + {}^3P_1$ ($f = 1/2$) state. The measured fraction of the remaining atoms' signal is plotted vs the detuning from the $^1S_0 + {}^3P_1$ ($f = 1/2$) asymptote. Each data point is an average of six measurements and the solid lines are fitted Lorentz profiles. PA laser intensities are adjusted to give a comparable atom loss for all spectra, ranging from 3.6 to 1067 mW/cm^2, respectively.

III. SYSTEMATIC SHIFTS AND PA DETUNINGS

The systematic frequency shifts and associated systematic uncertainty are estimated to get accurate PA frequency detuning. The dominated systematic frequency shifts are induced by the PA light, atomic temperature, and the optical lattice. The frequency shift induced by the PA laser is related to the Franck-Condon factors and the PA light intensity. We measure the PA transition frequency with several PA laser intensities and the shift can be estimated by extrapolation at zero intensity. An example of frequency shift by the PA lasers as a function of laser intensity is shown in Fig. 3(a). Due to the varying power of the PA light and transition intensities for different observed spectral lines, the PA light-induced shifts for all the spectra including the resonance line are measured
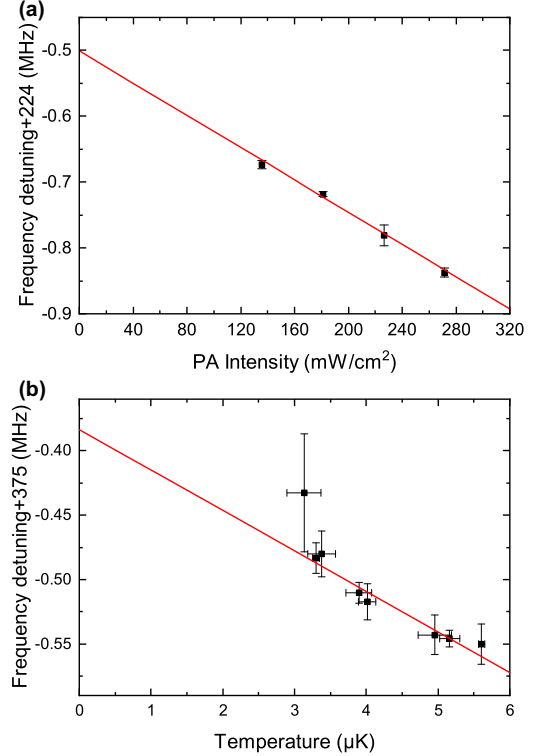

FIG. 3. Frequency shift measurements. (a) An example of PA frequency shift induced by the PA laser as a function of laser intensity related to the 0^+ state. (b) Frequency shift induced by the temperature of atom samples that measured with the PA spectroscopy also related to the 0^+ state. Each data point is an average of six measurements and the solid line represents the linearly fitted profile.

and evaluated separately with the data summarized in Table I. The linear fitted slope data of the PA light shifts are given in Appendix B.

Before each PA spectra measurement, we also measure the $^1S_0 + {}^3P_1$ ($f = 1/2$) transition resonance frequency under the same optical lattice conditions which have almost the same optical lattice shift as the PA spectra [2]. Therefore, the optical lattice shifts of the PA frequency detuning from $^1S_0 + {}^3P_1$ ($f = 1/2$) resonance are approximately eliminated. Each measured PA spectrum results from a superposition of the spectra with different thermal collision energies of the atom pair, and as a result, the finite temperature induces a frequency shift [26]. The longitudinal temperature of atoms is measured by fitting the sideband spectrum of the 578-nm clock transition in the 759-nm magical wavelength optical lattices which is more accurate than the time-of-flight (TOF) method [27]. A 759-nm optical lattice has almost the same potential as the 780-nm lattice for ground-state atoms under the same optical intensity [28]. The temperature of the atoms in an optical lattice is approximately linearly related to the lattice potential depth [27]. We get the relationship between the lattice depth and atomic sample temperature by varying the lattice power. Subsequently, we measure the PA frequency detuning at several atomic sample temperatures, by setting different optical lattice powers. The PA frequency shift caused by temperature as a function of different temperatures is displayed in Fig. 3(b), with the lattice power varying from 0.55

to 0.95 W. The data corresponding to the lowest temperature deviate from the fitting line and exhibit a large uncertainty. This may be due to the low signal-to-noise ratio of PA spectroscopy at lower trap depths with a fewer number of atoms. The remaining lattice shift is included in the measurements of the temperature shift. We obtain a slope of 31.4 kHz/μK, which is in agreement with the value of $3k_B/2h$ [29]. This further confirms that the differences in lattice shifts between resonant transitions and PA transitions are negligibly small.

The density shift is measured through modulating the atom number in the lattice by varying the power of the 399-nm Zeeman cooling light. The frequency shift is about $-11(13)$ kHz for an operational atom number about 10^4. The density shift induced by variation of the atom number during the temperature shift estimate is comparably small and can be considered negligible. The Zeeman shift induced by environmental magnetism is theoretically estimated to be less than 1.4 kHz, which can be neglected. The statistical uncertainties are derived from multiple repeated measurements for each PA spectrum. The achieved statistical uncertainty of detuning is on the order of 10 kHz. All the PA frequency shifts and their associated uncertainties are outlined in Table I and the total uncertainty for each spectrum is within 100 kHz.

IV. EXCITED-STATE MOLECULAR POTENTIAL

These PA lines include contributions from the s-wave scattering ground state and the p-wave scattering ground state at our experiment temperature of about 6 μK. The lines associated with p-wave collisions are weak and the contribution from the other higher partial-wave states is not considered [20]. The observed PA spectra are classified into two groups based on the ground scattering states, s-wave and p-wave scattering states. Because the total wave function has to be antisymmetric for two fermionic atoms to exchange, s- and p-wave collisions occur for antisymmetric and symmetric atomic internal states. To determine the PA spectrum from which we obtain the initial scattering state, we implement spin polarization by optical pumping as in Ref. [24] before the PA process. As depicted in Fig. 4, the atom loss, which appears weaker compared to the unpolarized spectrum after spin polarization, is from the s-wave scattering state, while the unchanged spectrum arises from p-wave scattering. The persistence of the s-wave-related spectrum after spin polarization can be attributed to the imperfect pure spin polarization and inhomogeneous excitation. The population of the motion quantum states at finite temperature along with the nonideal homogenization of the PA light leads to the inhomogeneous excitation that gives rise to s-wave collisions [30–32].

Following the methods described in Refs. [20,33], the Hamiltonian for a diatomic molecule associated with the $^1S_0 + {}^3P_1$ ($f = 1/2$) atomic state can be represented as

$$H = \frac{p_r^2}{2\mu} + H_{\text{rot}} + H_{\text{BO}} + H_{\text{HF}}. \qquad (1)$$

The first two terms on the right-hand side represent the radial and angular kinetic energy of the atomic nuclei, respectively, in which μ and r denote the reduced mass and radial distance between the two nuclei. H_{BO} is the Born-Oppenheimer
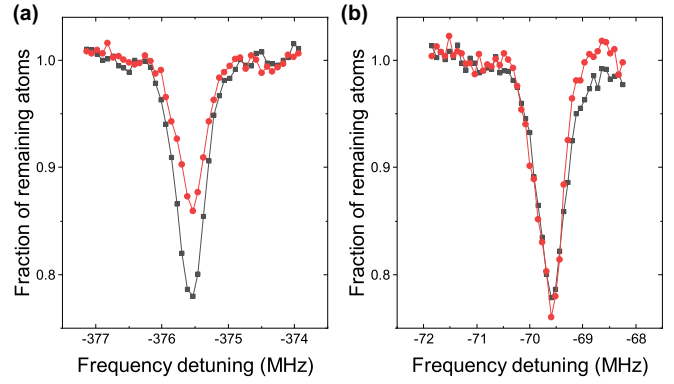

FIG. 4. The PA spectral lines from the (a) s-wave scattering ground state and (b) p-wave scattering ground state. The data from polarized and unpolarized atoms are represented by red circles and black squares, respectively, with each spectral line corresponding to the average result of six measurements.

(BO) potential that asymptotes to the $^1S_0 + {}^3P_1$ scattering channel including the dipole-dipole interaction and the van der Waals interaction. The BO potential is diagonal under Hund's case (c) and can be approximation written as

$$V_{\Omega\sigma}(r) = -sC_3^\Omega/r^3 - \frac{C_6}{r^6}\left(1 - \frac{\sigma^6}{r^6}\right), \qquad (2)$$

where $s = (-1)^{P+I}$ and P, I denote the spatial parity and total nuclear spin. Ω represents the projection of the total electronic angular momentum $\boldsymbol{J} = \boldsymbol{j}_1 + \boldsymbol{j}_2$ on the internuclear axis. The potential parameters in Eq. (2) are given in Ref. [34]. H_{HF} is the hyperfine coupling interaction term in the $^3P_1$ orbital which is diagonal in the Hund's case (e) base described by $a(\boldsymbol{i}_1 \cdot \boldsymbol{j}_1 + \boldsymbol{i}_2 \cdot \boldsymbol{j}_2)$, where a is the atomic hyperfine coupling constant [35]. The adiabatic potentials of ^{171}Yb$_2$ molecule correlating to the $^1S_0 + {}^3P_1$ atomic state can be obtained by diagonalizing the Hamiltonian in Eq. (1) via a basis transformation between different Hund's cases. The calculated adiabatic potentials at every position r for nonrotating excited molecular states are shown in Fig. 5. The allowed optical coupling of colliding atoms divides the excited molecular potential into two classes with even ($P = 0$) and odd ($P = -1$) parity. The axial projection ϕ of the angular momentum $\boldsymbol{F} = \boldsymbol{I} + \boldsymbol{J}$ is a good quantum number. The potentials are labeled by ϕ, and the superscript indicates the reflection symmetry with respect to a plane containing the molecular axis. The total angular momentum for two atoms denoted as $\boldsymbol{T}$ that represents the sum of $\boldsymbol{F}$ and the rotation $\boldsymbol{R}$. The p-wave ($T = 0, 1, 2$) and s-wave ($T = 0$) ground-state scattering states have odd and even spatial parity, respectively. According to the selection rules, the excited states associated with s-wave collisions must have odd parity and $T = 1$ while the excited states associated with p-wave collisions have even parity and $T = 0, 1, 2, 3$.

According to the molecular potentials from diagonalizing the Hamiltonian in Eq. (1), we compute the bound-state energy levels by the discrete variable representation (DVR) method [36]. The calculated result ν_{theor} and experimental data ν_{expt} are shown in Table I. Some states are not observed in experiment, which may have a small Frank-Condon
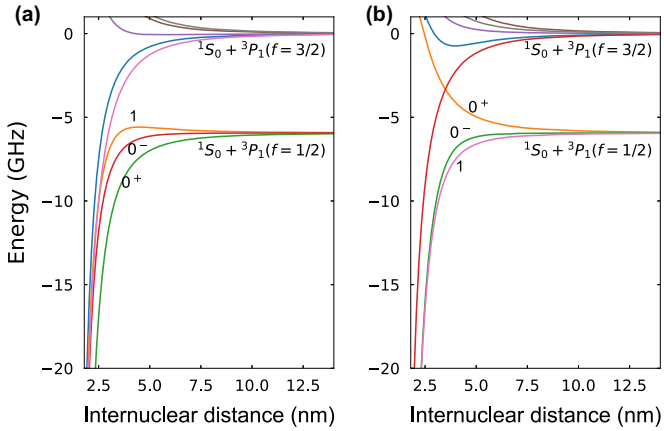
FIG. 5. Adiabatic potentials near the $^1S_0 + {}^3P_1$ dissociation limit. Excitation states of atoms for the (a) nuclear spin-singlet s-wave collision ground states and (b) nuclear spin-triplet p-wave collision ground states.

factor. By comparing and analyzing theoretical results based on the adiabatic molecular potential with experimental data, we clarify the excited molecular potential corresponding to the spectral lines. Some spectral lines show significant discrepancies between experimental and theoretical results. The excited molecular potentials are not assigned for those spectral lines which need further theoretical investigation and accurate model calculation. The excited molecular potential states for PA lines are labeled in Table I. Most of the spectra related to s-wave scattering ground states correspond to the 0^+ excited molecular potential and most of the spectra-related p-wave scattering ground states correspond to the $|\phi| = 1$ excited molecular potential.

V. CONCLUSION

In conclusion, we present high-accuracy PA spectra of ^{171}Yb atoms near the dissociation limit of the $^1S_0 + {}^3P_1$ ($f = 1/2$) hyperfine transition in an optical lattice. The main systematic frequency shifts of the PA transitions are determined achieving total uncertainties of less than 100 kHz. The initial collision states of the PA spectra are investigated by comparing the spectra with and without spin polarizing. Then we calculate the bound-state energy levels and assign the excited molecular state for spectral lines. PA spectra of cold ^{171}Yb atoms near the intercombination line provide an important foundation for studying the collisional properties between atoms and investigating more novel quantum phenomena using ^{171}Yb atoms. This research lays the groundwork for efficient photoassociative production of cold ytterbium molecules and the exploration of dissipative many-body systems.
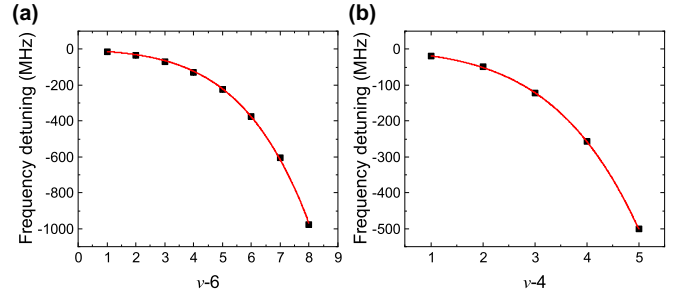
FIG. 6. The measured PA frequency detuning. (a) PA detuning related to the 0^+, $P = -1$ excited molecular potential. (b) PA frequency detuning related to the $|\phi| = 1, T = 2, P = 0$ excited molecular potential. The solid lines represent the fitting profile.

APPENDIX A: FITTING OF THE MEASURED PA DETUNING

The measured PA frequency detuning data that related to the 0^+, $T = 1$ excited molecular potential with odd parity and the $|\phi| = 1$, $T = 2$ excited molecular potential with even parity are shown in Figs. 6(a) and 6(b), respectively. The data are approximately consistent with the semiclassical Leroy-Bernstein formula's from $E_\nu = [(\nu - \nu_D)H_3]^6$, where ν is the vibrational quantum number [37].

APPENDIX B: PA LIGHT SHIFT AND THE LINEWIDTHS OF PA SPECTRA

The data of linear fitted slopes of the PA laser-induced shifts and the linewidths of measured PA spectra are given in Table II.

APPENDIX C: INFLUENCE OF PA LIGHT POLARIZATION AND LATTICE FREQUENCY FLUCTUATIONS

The PA detuning from resonance frequency of $^1S_0 + {}^3P_1$ ($f = 1/2$) transition with different optical lattice frequencies is shown in Fig. 7(a). The variation of PA detuning is within the range of 100 kHz. The experiment is carried with a 780-nm optical lattice, in which the PA detuning is insensitive to variations of lattice frequency. The frequency shifts induced
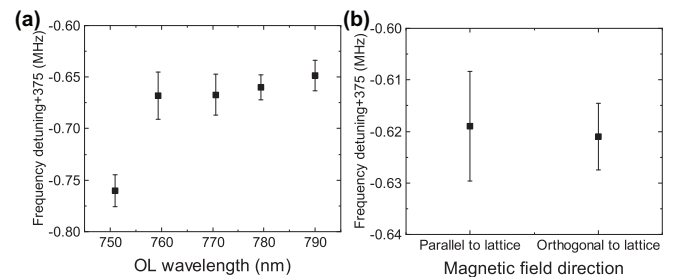

FIG. 7. Effects of lattice light frequency and PA light polarization. (a) PA frequency under several optical lattice frequencies. (b) The PA detuning under different polarized PA light.

TABLE II. Linear fitted slopes of the PA light shift and the linewidths of PA spectra.

PA resonance detuning (MHz)	Linear fitted slopes of PA shift (kHz/mW cm^2)	Linewidths of PA spectra (MHz)
−16.148(43)	−5.478(2121)	0.527(29)
−18.789(42)	−2.222(994)	0.772(33)
−21.484(43)	−3.826(1233)	0.780(39)
−34.93(41)	−3.651(194)	0.524(33)
−49.428(54)	−3.327(685)	0.711(146)
−54.026(55)	−2.814(44)	0.653(55)
−69.219(47)	0.610(56)	0.637(25)
−79.900(42)	−0.872(264)	0.352(13)
−115.287(62)	−1.793(71)	0.642(97)
−122.648(54)	−1.593(41)	0.615(87)
−128.049(45)	−1.223(76)	0.643(4)
−224.27(43)	−0.449(153)	0.614(9)
−245.403(6)	−0.431(71)	0.617(72)
−256.548(47)	−0.580(33)	0.581(52)
−375.234(43)	−0.165(26)	0.608(25)
−484.477(6)	−0.248(18)	0.796(121)
−500.466(52)	−0.342(24)	0.645(54)
−603.807(42)	−0.002(3)	0.536(4)
−887.576(43)	−0.181(4)	0.482(18)
−975.543(43)	−0.181(4)	0.647(24)

by lattice frequency fluctuations can be safely ignored under our experimental conditions.

Finally, we compare the PA detuning under varying polarizations of PA light by adjusting the quantum axis direction using a magnetic field that is either parallel to or orthogonal to the optical lattice. The experimental results indicate that there is no difference under our measurement accuracy [Fig. 7(b)].

[1] K. M. Jones, E. Tiesinga, P. D. Lett, and P. S. Julienne, Rev. Mod. Phys. **78**, 483 (2006).

[2] M. Kitagawa, K. Enomoto, K. Kasa, Y. Takahashi, R. Ciuryło, P. Naidon, and P. S. Julienne, Phys. Rev. A **77**, 012719 (2008).

[3] K. Enomoto, M. Kitagawa, K. Kasa, S. Tojo, and Y. Takahashi, Phys. Rev. Lett. **98**, 203201 (2007).

[4] K. Enomoto, K. Kasa, M. Kitagawa, and Y. Takahashi, Phys. Rev. Lett. **101**, 203201 (2008).

[5] T. L. Nicholson, S. Blatt, B. J. Bloom, J. R. Williams, J. W. Thomsen, J. Ye, and P. S. Julienne, Phys. Rev. A **92**, 022709 (2015).

[6] M. Yan, B. J. DeSalvo, B. Ramachandhran, H. Pu, and T. C. Killian, Phys. Rev. Lett. **110**, 123201 (2013).

[7] F. K. Fatemi, K. M. Jones, and P. D. Lett, Phys. Rev. Lett. **85**, 4462 (2000).

[8] K.-K. Ni, S. Ospelkaus, M. H. G. De Miranda, A. Pe'er, B. Neyenhuis, J. J. Zirbel, S. Kotochigova, P. S. Julienne, D. S. Jin, and J. Ye, Science **322**, 231 (2008).

[9] W. Skomorowski, R. Moszynski, and C. P. Koch, Phys. Rev. A **85**, 043414 (2012).

[10] G. Cappellini, L. F. Livi, L. Franchi, D. Tusi, D. Benedicto Orenes, M. Inguscio, J. Catani, and L. Fallani, Phys. Rev. X **9**, 011028 (2019).

[11] M. S. Safronova, D. Budker, D. DeMille, D. F. Jackson Kimball, A. Derevianko, and C. W. Clark, Rev. Mod. Phys. **90**, 025008 (2018).

[12] T. Tomita, S. Nakajima, I. Danshita, Y. Takasu, and Y. Takahashi, Sci. Adv. **3**, e1701513 (2017).

[13] S. L. Campbell, R. B. Hutson, G. E. Marti, A. Goban, N. Darkwah Oppong, R. L. McNally, L. Sonderhouse, J. M. Robinson, W. Zhang, B. J. Bloom, and J. Ye, Science **358**, 90 (2017).

[14] W. F. McGrew, X. Zhang, R. J. Fasano, S. A. Schäffer, K. Beloy, D. Nicolodi, R. C. Brown, N. Hinkley, G. Milani, M. Schioppo, T. H. Yoon, and A. D. Ludlow, Nature (London) **564**, 87 (2018).

[15] L. F. Livi, G. Cappellini, M. Diem, L. Franchi, C. Clivati, M. Frittelli, F. Levi, D. Calonico, J. Catani, M. Inguscio, and L. Fallani, Phys. Rev. Lett. **117**, 220401 (2016).

[16] Z. Ren, D. Liu, E. Zhao, C. He, K. K. Pak, J. Li, and G.-B. Jo, Nat. Phys. **18**, 385 (2022).

[17] S. Ma, A. P. Burgers, G. Liu, J. Wilson, B. Zhang, and J. D. Thompson, Phys. Rev. X **12**, 021028 (2022).

[18] A. Jenkins, J. W. Lis, A. Senoo, W. F. McGrew, and A. M. Kaufman, Phys. Rev. X **12**, 021027 (2022).

[19] Y. Takasu, K. Komori, K. Honda, M. Kumakura, T. Yabuzaki, and Y. Takahashi, Phys. Rev. Lett. **93**, 123202 (2004).

[20] K. Enomoto, M. Kitagawa, S. Tojo, and Y. Takahashi, Phys. Rev. Lett. **100**, 123001 (2008).

[21] J. H. Han, J. H. Kang, M. Lee, and Y. Shin, Phys. Rev. A **97**, 013401 (2018).

[22] R. Yamazaki, S. Taie, S. Sugawa, and Y. Takahashi, Phys. Rev. Lett. **105**, 050405 (2010).

[23] Q. Gao, M. Zhou, C. Han, S. Li, S. Zhang, Y. Yao, B. Li, H. Qiao, D. Ai, G. Lou, M. Zhang, Y. Jiang, Z. Bi, L. Ma, and X. Xu, Sci. Rep. **8**, 8022 (2018).

[24] L. Luo, H. Qiao, D. Ai, M. Zhou, S. Zhang, S. Zhang, C. Sun, Q. Qi, C. Peng, T. Jin, W. Fang, Z. Yang, T. Li, K. Liang, and X. Xu, Metrologia **57**, 065017 (2020).

[25] R. Ciuryło, E. Tiesinga, and P. S. Julienne, Phys. Rev. A **71**, 030701(R) (2005).

[26] T. Zelevinsky, M. M. Boyd, A. D. Ludlow, T. Ido, J. Ye, R. Ciuryło, P. Naidon, and P. S. Julienne, Phys. Rev. Lett. **96**, 203201 (2006).

[27] C. Han, M. Zhou, X. Zhang, Q. Gao, Y. Xu, S. Li, S. Zhang, and X. Xu, Sci. Rep. **8**, 7927 (2018).

[28] Z.-M. Tang, Y.-M. Yu, J. Jiang, and C.-Z. Dong, J. Phys. B: At. Mol. Opt. Phys. **51**, 125002 (2018).

[29] S. Moal, M. Portier, J. Kim, J. Dugué, U. D. Rapol, M. Leduc, and C. Cohen-Tannoudji, Phys. Rev. Lett. **96**, 023203 (2006).

[30] S. Blatt, J. W. Thomsen, G. K. Campbell, A. D. Ludlow, M. D. Swallows, M. J. Martin, M. M. Boyd, and J. Ye, Phys. Rev. A **80**, 052703 (2009).

[31] N. D. Lemke, J. von Stecher, J. A. Sherman, A. M. Rey, C. W. Oates, and A. D. Ludlow, Phys. Rev. Lett. **107**, 103902 (2011).

[32] A. D. Ludlow and J. Ye, C. R. Phys. **16**, 499 (2015).

[33] I. Reichenbach, P. S. Julienne, and I. H. Deutsch, Phys. Rev. A **80**, 020701(R) (2009).

[34] M. Borkowski, R. Ciuryło, P. S. Julienne, S. Tojo, K. Enomoto, and Y. Takahashi, Phys. Rev. A **80**, 012715 (2009).

[35] P. E. Atkinson, J. S. Schelfhout, and J. J. McFerran, Phys. Rev. A **100**, 042505 (2019).

[36] E. Tiesinga, C. J. Williams, and P. S. Julienne, Phys. Rev. A **57**, 4257 (1998).

[37] R. J. LeRoy and R. B. Bernstein, J. Chem. Phys. **52**, 3869 (1970).